Article

Cell Reports

T-type Calcium Channel Regulation of Neural Tube Closure and EphrinA/EPHA Expression

Graphical Abstract

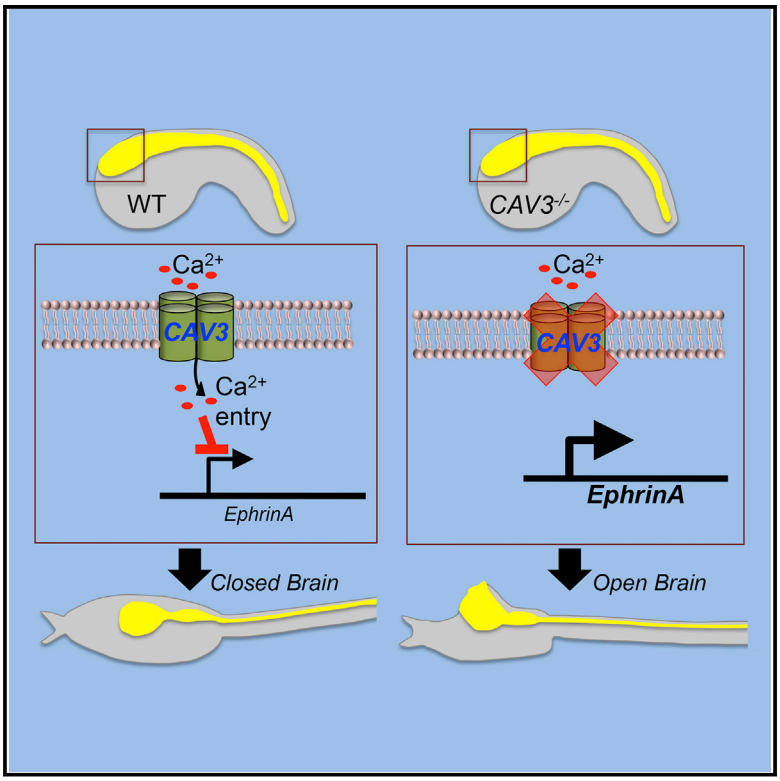

Authors

Sarah Abdul-Wajid, Heidi Morales-Diaz, Stephanie M. Khairallah, William C. Smith

Correspondence

william.smith@lifesci.ucsb.edu

In Brief

Abdul-Wajid et al. demonstrate a conserved requirement for T-type calcium channels in neural tube closure. The results describe how neural fold fusion is disrupted in T-type calcium channel mutants and morphants via misregulation of EphrinA effectors.

Highlights

- T-type calcium channels are required for neural tube closure in *Ciona* and *Xenopus*
- T-type calcium channels repress EphrinA expression in neural tube closure

Abdul-Wajid et al., 2015, Cell Reports *13*, 829–839
October 27, 2015 ©2015 The Authors
http://dx.doi.org/10.1016/j.celrep.2015.09.035

Cell Reports
Article

T-type Calcium Channel Regulation of Neural Tube Closure and EphrinA/EPHA Expression

Sarah Abdul-Wajid,[1] Heidi Morales-Diaz,[1] Stephanie M. Khairallah,[1] and William C. Smith[1,*]
[1]Department of Molecular, Cell and Developmental Biology, and Neuroscience Research Institute, University of California, Santa Barbara, Santa Barbara, CA 93106, USA
*Correspondence: william.smith@lifesci.ucsb.edu
http://dx.doi.org/10.1016/j.celrep.2015.09.035

SUMMARY

A major class of human birth defects arise from aberrations during neural tube closure (NTC). We report on a NTC signaling pathway requiring T-type calcium channels (TTCCs) that is conserved between primitive chordates (*Ciona*) and *Xenopus*. With loss of TTCCs, there is a failure to seal the anterior neural folds. Accompanying loss of TTCCs is an upregulation of EphrinA effectors. Ephrin signaling is known to be important in NTC, and ephrins can affect both cell adhesion and repulsion. In *Ciona, ephrinA-d* expression is downregulated at the end of neurulation, whereas, with loss of TTCC, *ephrinA-d* remains elevated. Accordingly, overexpression of *ephrinA-d* phenocopied TTCC loss of function, while overexpression of a dominant-negative Ephrin receptor was able to rescue NTC in a *Ciona* TTCC mutant. We hypothesize that signaling through TTCCs is necessary for proper anterior NTC through downregulation of ephrins, and possibly elimination of a repulsive signal.

INTRODUCTION

Neurulation, the process that transforms the neural plate into the neural tube, is a hallmark of the chordates. Although the details of neural tube closure (NTC) vary between species (Harrington et al., 2009), broadly conserved cytoskeletal mechanisms bring together the two lateral edges of the neural plate followed by their fusion at the dorsal midline. Disruption of NTC cellular mechanisms, such as those generating apically polarized constrictions in the epithelial neural plate cells, causes severe and sometimes irreparable defects in the spinal cord and brain (Haigo et al., 2003; Ybot-Gonzalez and Copp, 1999). Similarly, mutations that disrupt the planar cell polarity pathway genes, such as *dishevelled* and *vangl2*, have been shown to disrupt convergent extension movements necessary for NTC (Murdoch et al., 2001; Wallingford and Harland, 2001). The final step of NTC is neural fold adhesion and fusion, and some key factors, such as the products of the *grhl2* and *N-cadherin* genes, have been found through reverse and forward genetic approaches (Bronner-Fraser et al., 1992; Pyrgaki et al., 2011).

Despite the wealth of studies, our understanding of NTC remains incomplete and insufficient to explain the spectrum of human NTC defects (Greene and Copp, 2014; Wallingford et al., 2013). We describe a regulatory step in NTC that requires signaling through T-type calcium (Ca^{2+}) channels (TTCCs) for proper fusion of the closing neural tube. The requirement for T-type Ca^{2+} signaling appears to be late in NTC, and is distinct from earlier Ca^{2+} signaling events that are required for neural plate induction (Hackley et al., 2013; Leclerc et al., 2012), as well as from mechanisms of cell polarity and cytoskeletal-driven neural plate folding.

The original observation of the requirement for TTCCs in chordate NTC came from mapping analysis of mutant, *bugeye* (*bug*) in the ascidian *Ciona savignyi* (Abdul-Wajid et al., 2014). Here, we extend these observations from *C. savignyi* and show conservation of this gene function during NTC in the amphibian *Xenopus laevis*.

RESULTS

Loss of CAV3 Results in an Open Anterior Neural Tube

In a screen for spontaneous mutants in wild-collected *Ciona savignyi* (Veeman et al., 2011), we identified a recessive line (*bugeye*) with an open brain phenotype and mapped the causative mutation to the *cis*-regulatory region of the single TTCC gene (CAV3) of the *C. savignyi* genome (Abdul-Wajid et al., 2014). Further experiments showed that the expression level of CAV3 was greatly reduced in homozygous *bug* mutants relative to their wild-type siblings, suggesting that deficient Ca^{2+} signaling through the CAV3 channel was responsible for the open brain phenotype. To investigate this possible causative link further, the CAV3 gene in the closely related species *Ciona intestinalis* was targeted with CRISPR/Cas9 genome editing (Ran et al., 2013). Like *C. savignyi*, *C. intestinalis* has only a single CAV3 gene (Okamura et al., 2005). We targeted the *C. intestinalis* CAV3 gene using two guide RNAs complementary to exon 3 and 49. Nuclear Cas9 was expressed using the ubiquitous EF1alpha promoter (Stolfi et al., 2014). The eggs also received the plasmid ETR1 > H2B:GFP to mark cells of the CNS (Veeman et al., 2010). At the late tail-bud stage, a *bugeye(bug)-like* phenotype (i.e., open brain) was observed in 17% of the electroporated embryos (n = 362) versus 3% (n = 374) of embryos receiving a control guide RNA (Figures 1A and 1B) ($p = 0.0001$, Fisher's exact test). If both CAV3 guide RNAs cleaved the target sequence successfully, an expected deletion of ~23 kb of DNA from

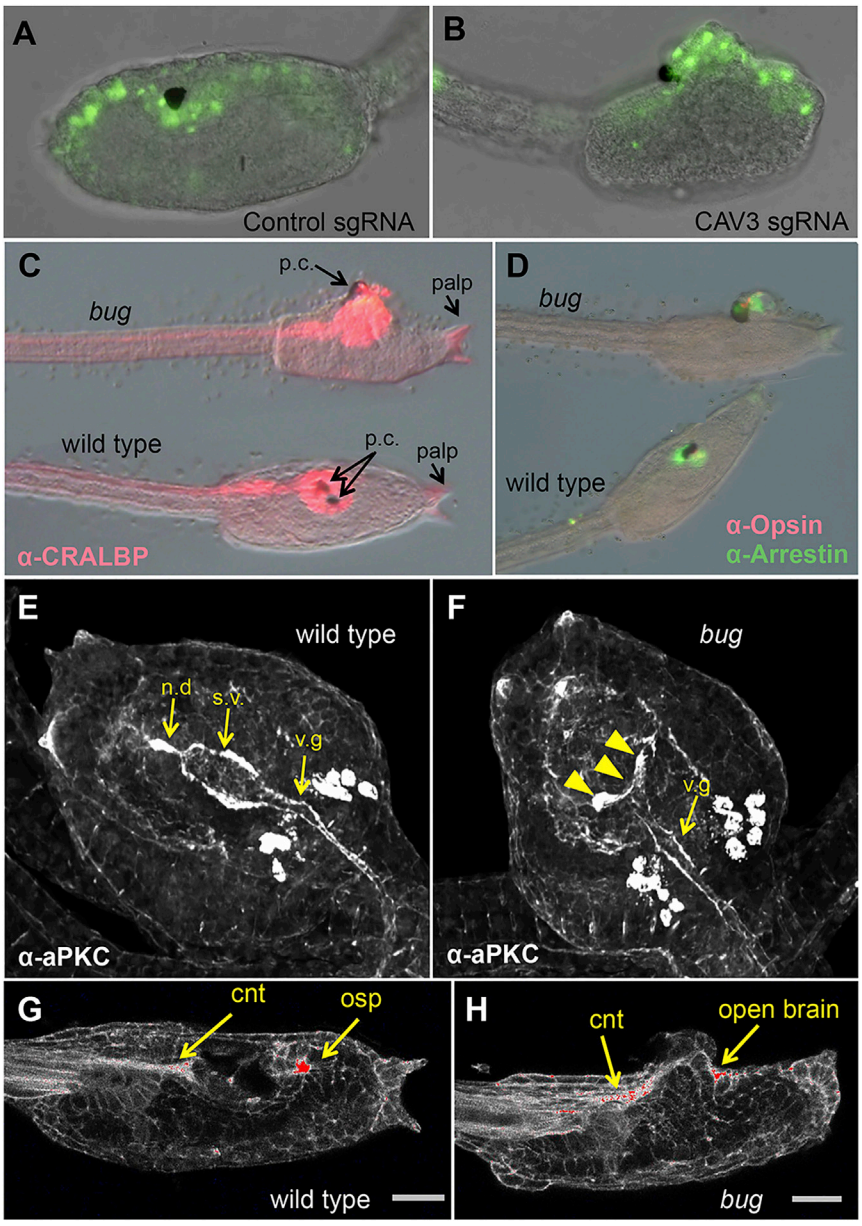

Figure 1. CAV3 Is Required for *Ciona intestinalis* Neural Tube Closure

(A and B) Representative *C. intestinalis* embryos expressing a control guide RNA (sgRNA) (A) or guide RNAs targeting exons 3 and 49 of the *C. intestinalis* CAV3 gene (CAV3 sgRNA) (B). See also Figure S1. Green fluorescence from a pan-neural ETR1 promoter driving nuclear GFP construct marks neural tube cells.

(C and D) *Bug* mutants differentiate and polarize the anterior neural tube. *Bugeye* (*bug*) and wild-type siblings were stained for the neural markers CRALBP, Opsin, and Arrestin, as indicated.

(E and F) Immunostaining for the cell polarity marker aPKC in wild-type and *bug* mutants. s.v., sensory vesicle; n.d., neurohypophyseal duct; v.g., visceral ganglion. The staining intensity is consistent between *bug* and wild-type, although the sensory vesicle in *bug* embryos is open (arrowheads in F). Views are dorsal.

(G and H) Phalloidin staining of *bug* and wild-type sibling larvae.

The most intense staining is in red. cnt, caudal neural tube; osp, oral siphon primordium. Scale bar, 24 μm.

C. intestinalis CAV3 gene would be produced. Using PCR primers spanning the outer edges of the target sites, an ~130-bp PCR product was detected in the *bug-like C. intestinalis* embryos, but not in the control guide RNA electroporated embryos (Figure S1A). Sequences of several cloned PCR products confirmed they were generated from the targeted region, and that they contained large and variable deletions (Figure S1B).

CNS Cells in the Bug Mutant Are Differentiated and Polarized

NTC defects, whether genetic or environmental, can be placed into two broad, and non-mutually exclusive, categories: those that arise from failure of neural tube differentiation and those that arise due to defects in the mechanics of neural tube folding and/or adhesion (Wallingford et al., 2013). In *C. intestinalis*, we previously characterized the mutant *frimousse*, which causes severe defects to the anterior neural tube, including a failure in brain closure (Deschet and Smith, 2004; Hackley et al., 2013). This mutation, the product of a lesion in a connexin gene, results from a failure to maintain neural induction in the anterior neural plate and is evident in the loss of expression of anterior CNS genes, and in the aberrant expression of an epidermal gene in the mis-specified brain. In contrast to *frimousse*, in *bug*, we observed comparable immunostaining of the pan-neural protein CRALBP, and the brain-specific proteins Opsin and Arrestin (Tsuda et al., 2003) in wild-type and mutant larvae (Figures 1C and 1D). In addition to the CNS, the adhesive palps in *bug* mutants were indistinguishable from wild-type. In *Ciona*, the palps are derived from the anterior-most region of the neural plate (Nishida, 1987; Veeman et al., 2010), and in *frimousse* embryos they are absent.

Mechanically, NTC is characterized by the formation of apically polarized actin filaments. The action of these polarized filaments results in the apical constriction of the cells and the folding of the neural plate inward. Disruption of this actin machinery and/or accessory proteins can cause neural tube closure defects (Wallingford, 2005). In *C. savignyi*, we observed that antibody staining for the apically localized cell polarity protein aPKC (Ghosh et al., 2008; Solecki et al., 2006) labels the surface of the CNS lumen (Figure 1E). In the *C. savignyi* brain periluminal

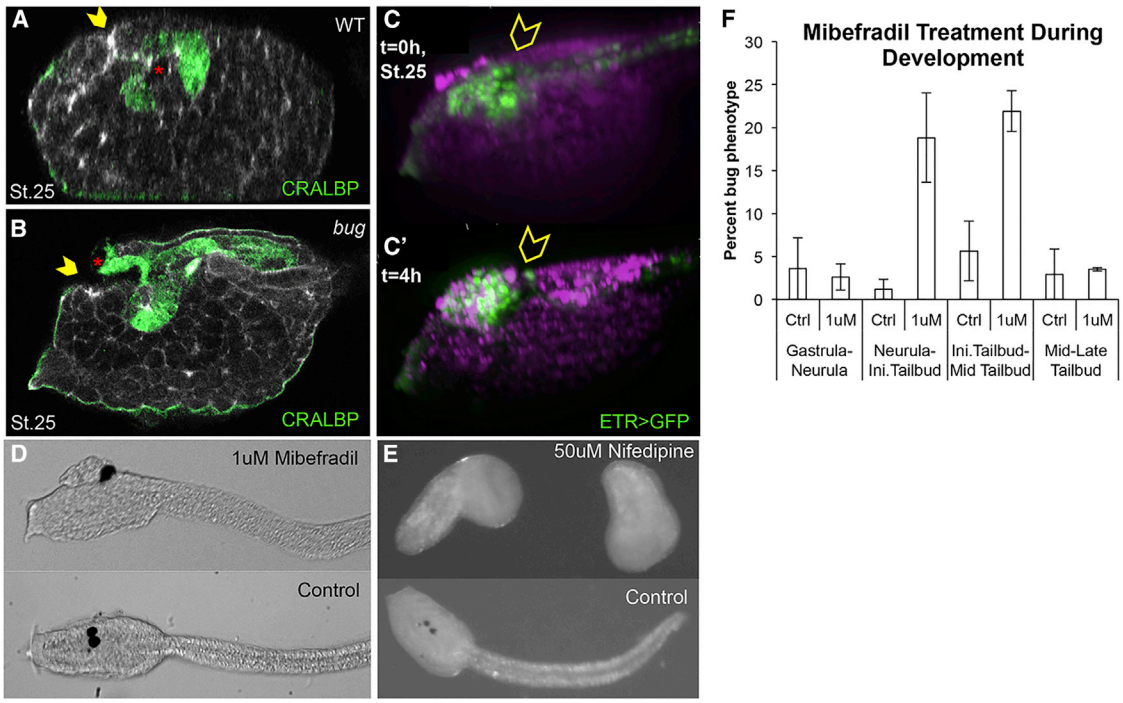

Figure 2. Onset of Open Brain Phenotype in *Ciona*

(A and B) Mid-sagittal confocal sections of late tail-bud (stage 25) *bug* and wild-type (WT) sibling embryos showing immunostaining for CRALBP. Yellow arrowheads indicate the anterior neuropore. The pigmented cells of the sensory vesicle are indicated by red asterisks.

(C and C′) Still images from the start and end of Movie S1 of a *bug* embryo. Cells of the neural tube express GFP from the pan-neural ETR1 promoter. Magenta indicates FM464-stained membranes. Yellow arrowheads indicate a sensory vesicle that, at the start of movie (C; t = 0), is covered by non-neural tissue (i.e., epidermis) and then at 4 hr (C′; t = 4 hr) is exposed on the surface.

(A–C′) Lateral view of head region with palps and anterior to the left).

(D) Treatment with mibefradil during neurulation phenocopies the *bug* phenotype.

(E) Treatment with nifedipine during neurulation stages causes an arrest in development.

(F) Mibefradil treatments. Dechorionated embryos at each developmental stage were subjected to control (water) or 1 μM mibefradil, washed after treatment, and then allowed to develop to swimming larvae stage. Percentage phenotype was calculated by counting the number of *bugeye*-like embryos over the total number of embryos treated. Error bars, SEM from three independent experiments.

staining can be seen in both the sensory vesicle and visceral ganglion (*Ciona* orthologs of the fore- and hindbrains, respectively), as well as in the neurohypophysial duct, which joins the sensory vesicle to the stomodeum (Manni et al., 2005). In *bug* mutants, we observed strong aPKC staining throughout the CNS, although anterior staining of the sensory vesicle was splayed outward in the open brain rather than forming a closed lumen (arrowheads in Figure 1F). Similarly, phalloidin labeling of *bug* mutants showed strong polarization of actin to the apices of cells in the CNS, including cells in the open anterior brain, of comparable intensity to phalloidin labeling in wild-type embryos (Figure 1G versus Figure 1H, red staining and yellow arrows). In summary, the CNS of *bug* mutants has no conspicuous defects in neural induction and specification, or in the formation of apically polarized cells.

Onset of Bug Phenotype

An important clue to the nature of the mechanism of the *bug* mutation comes from the observation that the phenotype, an open anterior neural tube, does not become apparent until after the late tail-bud stage, when neural tube closure in wild-type embryos is complete. At stage 25 (late tail-bud) sagittal confocal sections of *bug* embryos show that the anterior neural tube closure is largely complete, with most of the brain covered in epidermis, but with an enlarged anterior neuropore (yellow arrowheads in Figures 2A and 2B). Additionally, the two pigmented cells that comprise the ocellus and the otolith (Jiang et al., 2005) are misplaced in *bug* to the opening of the neuropore rather than in the brain vesicle (red asterisks in Figure 2B). To better visualize the developing CNS, the *bug* line was crossed with a stable transgenic line expressing GFP under the control of the pan-neural ETR1 promoter. Time-lapse movies of *bug* embryos confirm that the brain is initially covered with epidermis (i.e., relatively normal brain closure and neurulation), and that, over the course of approximately 4 hr, the brain erupts from the anterior neuropore by hatching larva stage (Figures 2C and 2C′; Movie S1). These data demonstrate that the late step of anterior neuropore sealing is defective in *bug* embryos (whereas earlier neurulation is normal), and that this results in the opening and protrusion of the initially epidermis-covered brain.

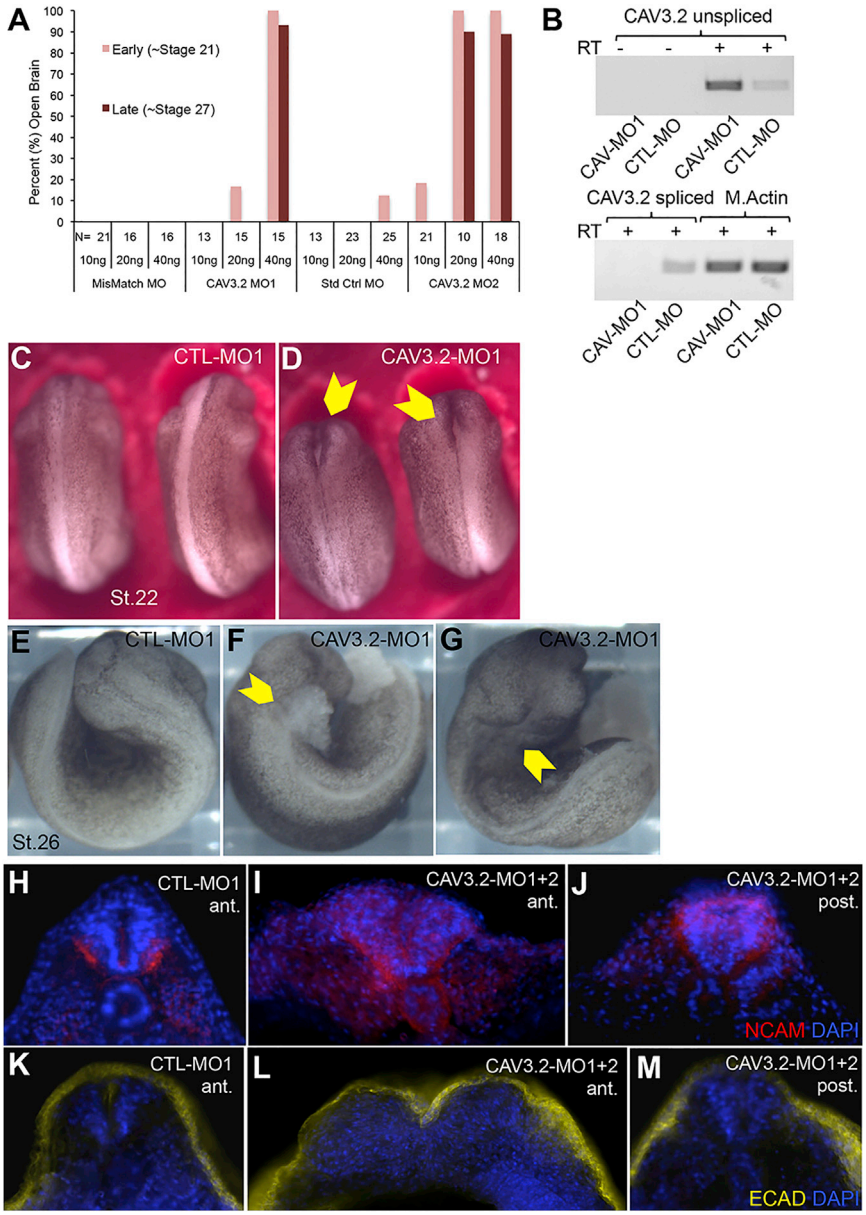

Figure 3. *X. laevis* CAV3.2 Morpholino Knockdown

(A) Quantification of MO knockdown phenotype at stages 21 and 27. Two MOs targeting *X. laevis* CAV3.2 (CAV3.2-MO1 and CAV3.2-MO2) and two control MOs (mismatch [CTL-MO1] and standard control [CTL-MO2]; see Experimental Procedures) were tested. The quantities of MO injected per embryo are indicated below the number (N) of embryos scored for each dose of MO.

(B) Disruption of CAV3.2 transcript splicing by CAV-MO1. RT-PCR was used to detect both the correct and expected splice-disrupted transcripts in cDNA samples from three pooled CTL-MO and three CAV-MO1-injected embryos. Muscle actin (M. Actin) RT-PCR was used to control for RNA load, and RT-minus controls are also shown.

(C and D) Early tail-bud stage embryos (stage 22) injected at the one-cell stage with a CTL-MO1 (C) or a CAV3.2-MO1 (D). Yellow arrowheads in (D) indicate anterior open neural tube.

(E–G) Tail-bud stage (stage 26) CTL-MO1- (E) and CAV3.2-MO1- (F and G) injected embryos. Anterior neural tube defects were observed in the CAV3.2-MO1 injections either with cellular matter erupting from the open neural tube (yellow arrowhead in F) or with a malformed head and deep dimple in the hindbrain (yellow arrowhead in G). See also Movie S2.

(H–J) NCAM staining (red) in anterior or posterior coronal sections of CTL-MO1- (H) and CAV3.2-MO1+2- (I and J) injected embryos.

(K–M) E-cadherin staining (yellow) in anterior and posterior coronal sections of CTL-MO1- (K) or CAV3.2-MO1+2- (L and M) injected embryos. MO-injected embryos used for sections were stage matched at approximately stage 24 based on somite development. All sections were also stained for nuclei (DAPI, blue).

Temporal T-type Ca^{2+} Channel Function

To better understand the temporal requirement for CAV3 in neural tube closure, embryos were treated at various time points with the TTCC-blocking drug mibefradil (Martin et al., 2000). Preliminary experiments confirmed that mibefradil treatment of neurulating embryos closely phenocopies *bug*, while the L-type channel blocker, nifedipine, gives a much different phenotype (Figures 2D and 2E). Treatment of embryos with mibefradil during short temporal windows identified the period of sensitivity for anterior neural tube closure: between neurula and midi tail-bud stages (Figure 2F). Thus, there is a lag time of ~5 hr from when CAV3 function is required (between stage 16 and 21) and the stage at which the phenotype becomes fully evident (stage 25 onward) suggesting an early tail-bud CAV3-dependent signal, which plays a role in the later sealing of the anterior neuropore.

Xenopus Requires a T-type Ca^{2+} Channel to Close the Anterior Neural Tube

X. laevis has three orthologs of *Ciona* CAV3: CAV3.1, 3.2, and 3.3. CAV3.2 is the earliest of these to be expressed in the neurulating embryo (Lewis et al., 2009). To determine whether this gene has a conserved role with its *Ciona* ortholog in neurulation, we used morpholino oligonucleotides (MO) to knock down its expression. Two splice-blocking MOs to *X. laevis* CAV3.2 were tested (CAV-MO1 and CAV-MO2), as well as two control MOs (standard control MO [Genetools] and custom mismatch MO). Both CAV3.2 MOs produced open brain phenotypes in 80%–100% of injected embryos (albeit at different dose efficacies), while no neurulation defects we observed with either control MO (Figure 3A). RT-PCR confirmed the efficacy of the MOs in blocking splicing and downregulation of spliced transcript (Figure 3B).

The defect caused by the CAV3.2 MOs can be seen in representative embryos at stage 22 as a failure of the anterior neural folds to fuse (Figures 3C and 3D). The defect is not simply a

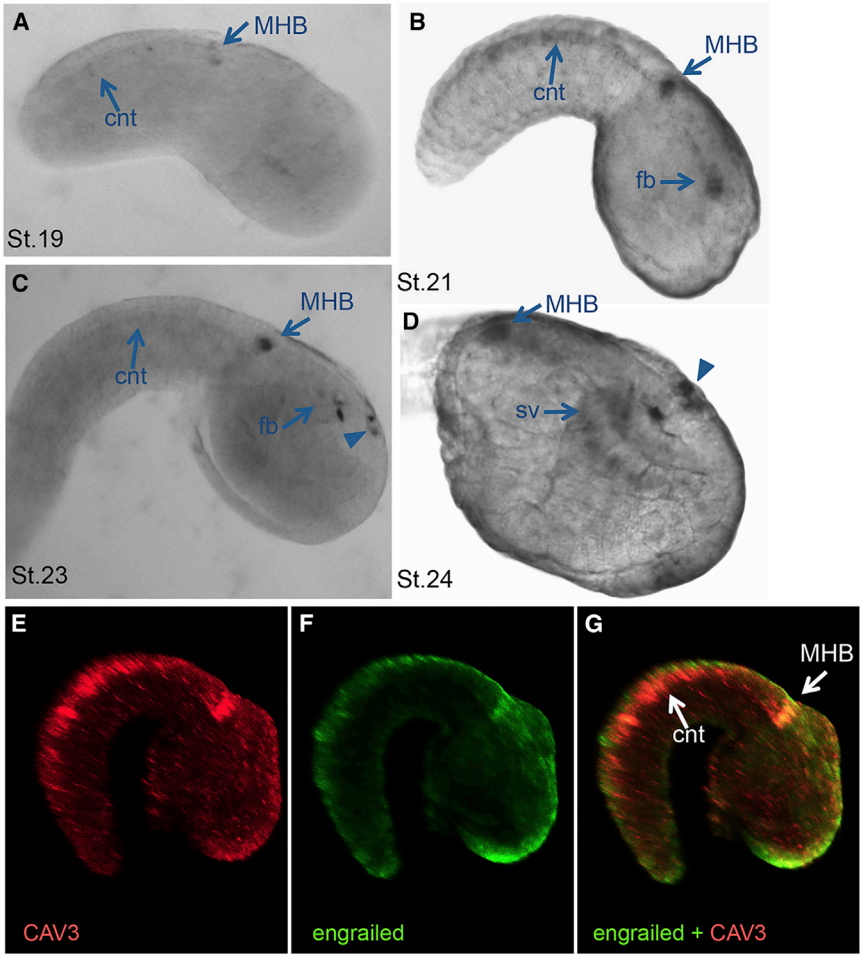

Figure 4. Expression of *C. savignyi* CAV3

(A–D) In situ hybridization of CAV3 expression in wild-type *C. savignyi* embryos. Expression is first detectable at early tail-bud stage (A; stage 19) in the midbrain-hindbrain (MHB) region and faintly in the caudal nerve cord (cnt). This expression intensified by mid tail-bud, and new expression in the forebrain (fb) is observed (B; stage 21). By late tail-bud (C and D) stage 23/24, new expression is seen in a cluster of cells in the epidermis (arrowheads) (sv, sensory vesicle).

(E–G) Double fluorescent in situ for CAV3 and engrailed yields overlapping expression at the MHB (but not in the cnt). Embryos are stage 22.

delay, as no fusion of the anterior folds is seen with extended culturing. In fact, by stage 26 we observed in 17% of 58 CAV-MO1-injected embryos that material (possibly brain) erupted from the open neural pore (Figures 3E and 3F; Movie S2). The remainder of the CAV3.2 MO1-injected embryos at stage 26 showed severe head malformations with a deep dimple at the hindbrain (Figure 3G).

As in the *Ciona bug* mutant, we observed no general defect in neural induction for *X. laevis* embryos injected with the CAV3.2 MOs based on NCAM antibody staining, although anterior closure was clearly defective (Figures 3H–3J; stage 24 embryos). Immunostaining for E-cadherin, which marks the epidermis in *X. laevis*, showed that even where the anterior neural tube was splayed open in the CAV3.2 MO embryos, an abnormal covering of epidermis was found over and into the open neural folds (Figures 3K–3M). These results demonstrate that *X. laevis* embryos also require a TTCC gene, CAV3.2, to effectively close, but apparently not to specify, the anterior neural tube.

CAV3 Expression in Ciona

The results above suggest a conserved functional role for TTCCs in chordate neural tube closure. To further examine conservation between the two genes, their spatial expression was compared.

The expression of the *X. laevis* CAV3.2 gene has already been described (Lewis et al., 2009). At developmental stages relevant for neural tube closure (as early as stage 20), *X. laevis* CAV3.2 expression is observed along the lateral edges of the developing neural folds and tube. This expression extends the length of the neural tube and increases into fore-, mid-, and hindbrain regions at later stages (24–36) as well as into the presumptive heart tissue (Lewis et al., 2009). For *C. savignyi*, the expression of the CAV3 gene was investigated by in situ hybridization. No specific signal could be detected until early tail-bud stage (*Ciona* stage 19 [Hotta et al., 2007]). At this stage, the most conspicuous hybridization was observed in a cluster of cells that appear to correspond to the midbrain-hindbrain boundary (MHB) region and in the caudal nerve cord (Figure 4A). Based on the conserved expression patterns of *otx*, *engrailed*, *pax2/5/8*, and *fgf8/17/18* in the brain, *Ciona* is thought to have a structure equivalent to the midbrain-hindbrain organizer (Raible and Brand, 2004). Expression of *C. savignyi* CAV3 increased in intensity in the MHB region at mid and late tail-bud stages, and new expression was observed both in the forebrain (arrows in Figures 4B–4D) and in a small patch of cells in the epidermis overlaying the sensory vesicle, posterior to the anterior neuropore (arrowheads in Figures 4C and 4D). Double fluorescent in situ hybridization confirms that the expression of *engrailed* and *CAV3* overlap in the *C. savignyi* MHB region (Figures 4E–4G).

Ca^{2+} Transients in Neurulating Embryos

Calcium transients in the developing neural plate and tube of both *Ciona* and *Xenopus* have been well documented. We described the presence of gap junction-dependent Ca^{2+} transients in the neural plate of *C. intestinalis* (Hackley et al., 2013), and in *Xenopus* Ca^{2+} transients via the DHP-sensitive CAV1 family play a critical role in neural induction (reviewed in Leclerc et al., 2012). However, TTCC transients in the neurulating chordate CNS have not been reported. To investigate this, one-cell stage *X. laevis* embryos were injected with the RNA encoding the Ca^{2+}

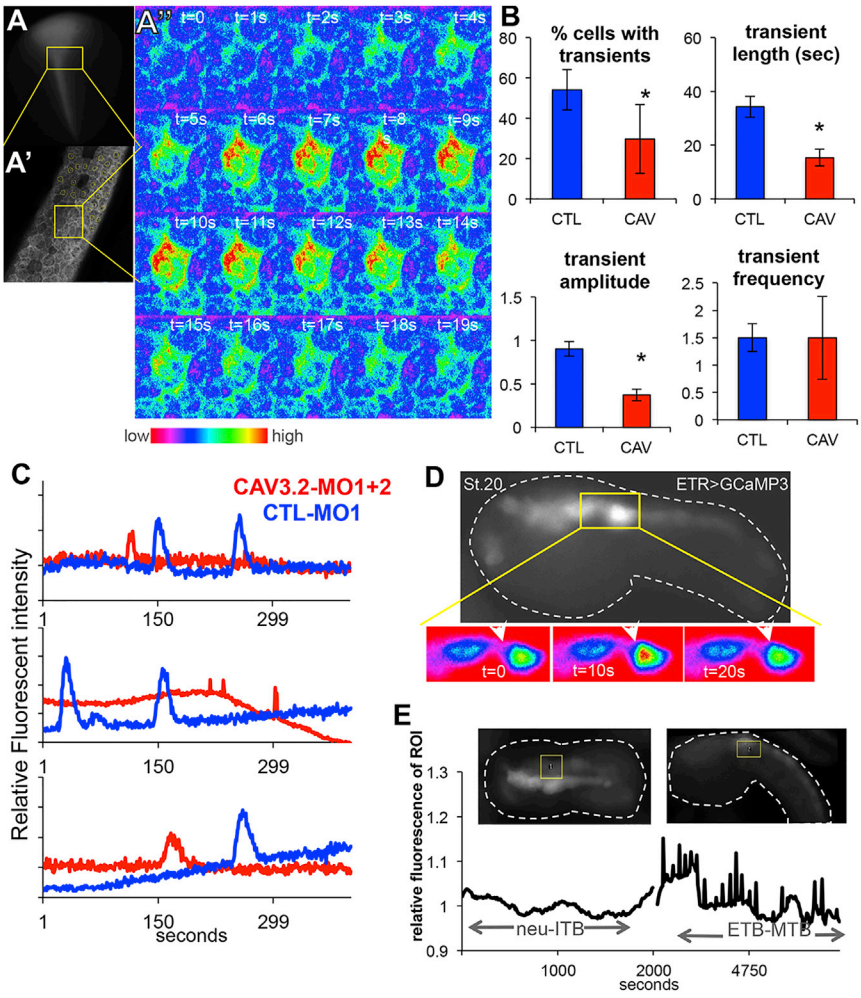

Figure 5. Calcium Transients in the Neural Tubes of *C. savignyi* and *X. laevis*

(A–A″) *Xenopus* embryo injected with GCaMP3 RNA shows Ca^{2+} transients during neurulation. Top left, a late neurula embryo expressing GCaMP3 in the closing neural tube (A). Low-magnification view of *X. laevis* embryo shows typical area recorded for Ca^{2+} transients (yellow box). Anterior is up. (A′) High magnification of the Z plane of the *X. laevis* anterior neural plate that was imaged. (A″) GCaMP fluorescence for a single cell in the neural plate undergoing a Ca^{2+} transient ($[Ca^{2+}]$ is indicated by color scale). See also Movies S3 and S4.

(B) CAV3.2 morpholino knockdown (CAV3.2-MO1, CAV) reduces the number of cells in the neural tube displaying Ca^{2+} transients and the length and amplitude of the transients, but not the frequency. The y axis in the amplitude graph shows relative fluorescent intensity (see Experimental Procedures). The frequency values are also described in Experimental Procedures. Control embryos were injected with a non-specific MO (CTL-MO2, CTL). Data represent quantification of three embryos from three independent experiments; error bars, SEM (*$p < 0.05$).

(C) Typical Ca^{2+} transients in CAV-MO knockdown and CTL-MO *X. laevis* neural tube cells.

(D) Ca^{2+} transients in *C. savignyi* embryos detected with GCaMP3 expressed from the pan-neural ETR1 promoter. Top panel shows one frame from a time-lapse movie. Lower panel is a close up of the midbrain hindbrain region (yellow box in top panel) showing a single Ca^{2+} transient with fluorescence intensity using the color scale from (A″). See also Movie S5.

(E) Time-lapse image of Ca^{2+} transients in the *C. savignyi* MHB region. Representative images from two time points (neurula and mid tail-bud) of an embryo expressing GCaMP3 with the MHB region of interest (ROI) are outlined in yellow. Dashed white lines outline the embryo. Bottom panels show relative fluorescence intensity in the ROI over time. Neu-iTB, neurula to initial tail-bud; ETB-MTB, early to mid tail-bud.

indicator GCaMP3 (Tian et al., 2009) and either control or CAV3.2 MOs. Live imaging was centered to the anterior closing neural folds of neurula stage embryos, where neural tube closure defects were observed and CAV3.2-expressing cells are present (Lewis et al., 2009). In a single plane of view of control MO embryos, we could detect Ca^{2+} transients in ~50% of the cells in the field of view, with each transient lasting on average 33 s (Figures 5A–5C; Movie S3). The number of cells having transients and the length and the intensity of the transients were reduced in CAV3.2 MO embryos (Figure 5B, asterisks indicate significance of $p \leq 0.05$, Movie S4). However, no difference was detected in the frequency of the transients (Figure 5B). Thus, CAV3.2 is required for normal Ca^{2+} transients in the developing *X. laevis* anterior neural tube.

At early tail-bud stages in *C. savignyi*, we observed a strong correlation between CAV3 expression and Ca^{2+} transients using an electroporated construct with the ETR1 driver for GCaMP3 (Hackley et al., 2013). Starting at early tail-bud stage, GCaMP3 Ca^{2+} transients were observed in the MHB region (Figure 5D and 5E; Movie S5) and continued through the mid tail-bud stage. The MHB transients diminish after mid tail-bud stage (data not shown).

T-type Ca^{2+} Channels and Ephrin Regulation

The characterization of the TTCC phenotypes in both *Ciona* and *Xenopus* suggest that the neural tube closure defects arises not from a deficiency in neural induction or neural tube folding, but rather from a later event, perhaps one involving cell adhesion and/or neuropore sealing. In mouse, EphrinA-EphA interactions have been shown to be important for neural fold fusion (Abdul-Aziz et al., 2009). We investigated expression levels of the *C. savignyi* ortholog of this gene, *ephrinA-d* (Picco et al., 2007), as well as neural cell adhesion molecule (NCAM), and the neural-specific genes *otx*, *six3/6*, and *etr1* (Takamura et al., 2001) at late tail-bud stages in wild-type and *bug* mutants by qRT-PCR . The ubiquitously expressed gene *RPS27A* was included as a control (Olinski et al., 2006). While there was no difference in expression of NCAM and ETR1 between wild-type and *bug*,

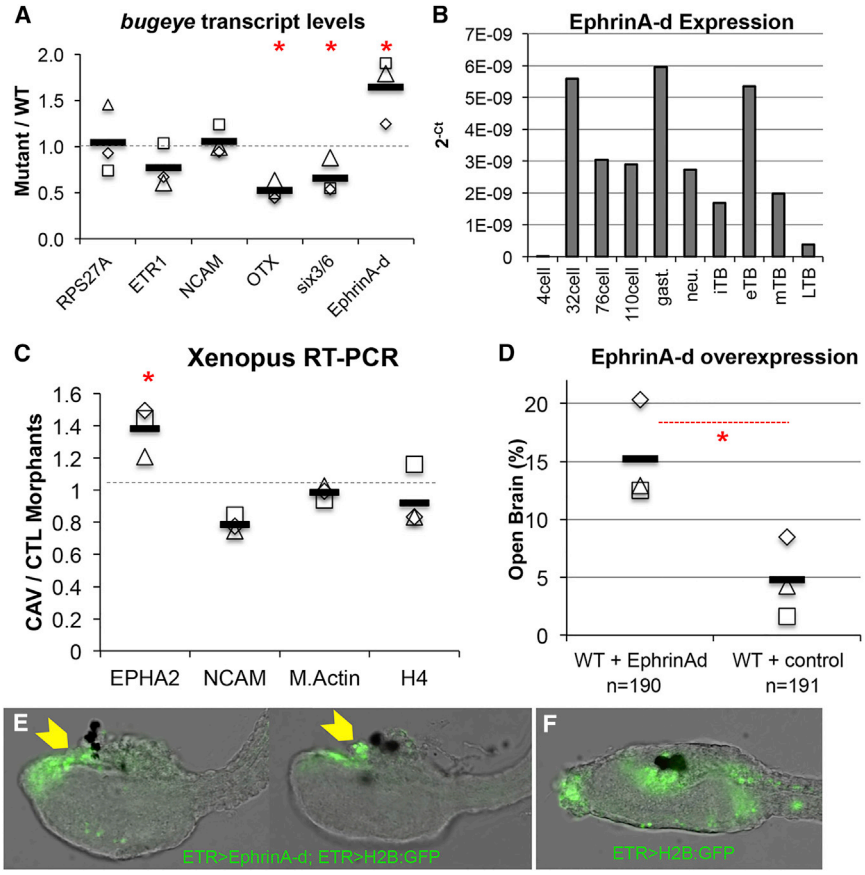

Figure 6. T-type Ca^{2+} Channel Regulation of EphrinA Signaling Components

(A) qRT-PCR assay for expression of the neural genes *etr1*, *otx*, *six3/6*, *NCAM*, and *ephrinA-d* in *bug* and wild-type (WT) larvae. ΔΔCT values were calculated by normalizing to the ubiquitously expressed gene *RPS27A* and then comparing to WT expression levels. The values for three independent biological repeats are indicated (open squares, etc.), as well as the average of the three (black bar). Red asterisks indicate significant difference between *bug* mutants and WT for given transcript; $p \leq 0.05$, t test. RPS27a values represent ΔCT comparison to WT.

(B) *C. savignyi* EphrinA-d transcript levels quantified over developmental time. qRT-PCR results are represented as log2(X) changes in absolute cycle threshold values for each developmental time point sample.

(C) RT-PCR for expression of *EPHA2*, *NCAM*, *M.Actin*, *and histone 4(H4)* in stage 24 *X. laevis* embryos were injected with either CAV3.2 splice disrupting morpholinos (CAV-MO1+2, CAV) or a control MO (CTL-MO2, CTL). The values for three independent biological repeats are indicated (open squares, etc.), as well as the average of the three (black bar). EPHA2 values are significantly different between CAV and CTL embryos (red asterisks, $p = 0.025$, standard t test).

(D) Percentage of open brain phenotype observed in WT embryos electroporated with either the EphrinA-d cDNA expression construct (WT+ EphrinAd) or H2B:GFP cDNA (WT+ control). Results from three independent trails are shown, as well as the average of the three (black bars). Red asterisks indicate significance, $p = 0.0006$, Fisher's exact test.

(E) EphrinA-d overexpression driven by pan-neural ETR promoter in *C. intestinalis* embryos phenocopies *bug*. Yellow arrowheads indicate the open brain. Two representative embryos are shown. The co-electroporated plasmid ETR > H2B:GFP labels the nervous system.

(F) Control embryo expressing only ETR > H2B:GFP.

ephrinA-d was upregulated approximately 1.6-fold in the mutant relative to wild-type. In these same *bug* embryos, we observed downregulation of the anterior neural genes *otx* and *six3/6* (Figure 6A). Because of the role of EphrinA in mouse neural tube closure and the similar expression patterns of *ephrinA-d* and *CAV3* (Imai et al., 2009), the *C. savignyi ephrinA-d* upregulation was of particular interest. In *C. intestinalis*, *ephrinA-d* has been shown to be necessary for the proper patterning of the neural plate, although a later role in neural tube closure has not been reported (Haupaix et al., 2014; Stolfi et al., 2011). We examined the normal developmental time course of *ephrinA-d* expression by qRT-PCR. Several peaks in *ephrinA-d* expression were observed: at 32-cell, gastrula and early tail-bud stages consistent with the previously published in situ data (Figure 6B) (Imai et al., 2009). Of potential significance is a dramatic downregulation of *ephrinA-d* expression from early through late tail-bud stages in wild-type embryos.

We also examined ephrinA signaling in *Xenopus* embryos. The ephrinA receptor EPHA2 is known to be expressed in the developing *X. laevis* neural tube (Brändli and Kirschner, 1995). A significant increase in the transcript for EPHA2 was observed in *X. laevis* embryos injected with the CAV3.2 MO relative to controls (Figure 6C, EPHA2 significance $p = 0.025$, t test), while no change was observed for *NCAM* expression (nor for *actin* and *histone 4*). While there are several EphrinBs expressed at this stage, their effects on the neural tube appears to be on apical constriction rather than adhesion (Ji et al., 2014).

To investigate whether mis-expressing EphrinA-d in *Ciona* in the late tail-bud *Ciona* embryos could replicate the *bug* phenotype, 1-cell stage embryos were electroporated with a plasmid containing the *ephrinA-d* cDNA driven by the ETR promoter, which expresses through the late tail-bud stage in *C. savignyi* (Tresser et al., 2010). A significant fraction of embryos electroporated with the EphrinA-d construct had an open brain phenotype compared to controls overexpressing nuclear GFP under the same promoter (15.2%, versus 4.8% in controls, $p = 0.0006$, Fisher's exact test) (Figures 6D and 6E versus 6F).

Rescue of Bug Embryos by ephrinA Inhibition

Based on the expression and overexpression data, we hypothesized that failure of *bug* embryos to properly downregulate *ephrinA-d* late in neurulation could cause the open-brain phenotype. To test this hypothesis directly, we asked whether inhibition of EphrinA-d could restore anterior neural tube closure in

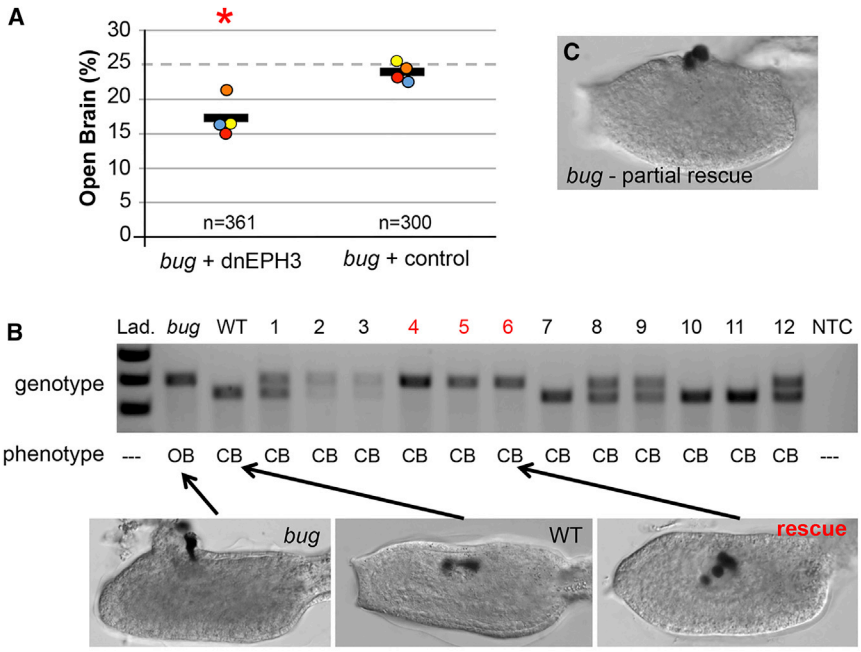

Figure 7. Rescue of *Ciona bugeye* Embryos with Dominant-Negative EPH3 (dnEPH3)

(A) Embryos from heterozygous *bug* parents were electroporated with either dnEPH3 driven by the pan-neural promoter ETR1 or an empty ETR1 vector (control). The fraction of embryos with the *bug* phenotype (open brain) was determined for each group. Circles represent the percentage of embryos showing the *bug* phenotype from four independent trials, and the black line is the average of the four trials (*n* is the combined number scored from the four trials). Red asterisks indicate significant p value of 0.002 using a chi-square test of deviation from the expected open brain frequency of 25%.

(B) Single tadpoles electroporated with dnEPH3 (lanes 1–12) and scored as having closed brains (CB) were genotyped with primers that distinguished the insertion-containing *bug* allele from the wild-type allele. The *bug* and wild-type (WT) lanes show the sizes the two alleles. Three of the 12 electroporated embryos (4–6, red) genotyped as homozygous for the *bug* allele despite having closed brains and are considered as rescued. Representative images of wild-type, *bug*, and rescued embryos are shown. See also Figure S2.

(C) Representative image of a partially rescued *bug* embryo.

bug embryos. For these experiments, a previously characterized dominant-negative version of the receptor for EphrinA-d, EPH3 (Picco et al., 2007; Haupaix et al., 2013), was expressed by electroporation in the CNS of *Ciona bugeye* embryos using the ETR1 promoter. Because the *bug* allele is lethal when homozygous (Abdul-Wajid et al., 2014), embryos are generated by crossing heterozygous adults. In clutches of *bug* embryos electroporated with the control plasmid, the *bug* phenotype was observed at close to the expected frequency of 25% (Figure 7A). In these experiments, four independent clutches of embryos were electroporated, and the frequency ranged from 23.1% to 25.4% (average 23.9%, n = 300, chi-square test, p = 0.689). In contrast, for embryos from the same clutches electroporated with the dominant-negative EPH3 (dnEPH3) the frequency of observed *bug* phenotypes ranged from 15% to 21% (average 17.1%, n = 361, chi-square test p = 0.002), indicating that anterior neural tube closure had been rescued in a portion of the *bug* embryos.

To further investigate the possible *bug* rescue, individual embryos were genotyped. The *bug* allele contains an 80-bp insertion that can readily be identified by gel electrophoresis of PCR-amplified genomic DNA from single embryos (Figure 7B). In a preliminary experiment, the link between the *bug* phenotype and the genomic insertion was confirmed (Figure S2). In 45 embryos examined, the *bug* phenotype was observed only in embryos homozygous for the insertion. Importantly, closed anterior neural tubes were never observed in those embryos homozygous for the insertion, nor were open neural tubes observed in those embryos genotyping as heterozygous, or genetically homozygous wild-type. For clutches electroporated with the dnEPH3 construct, 12 embryos scored as having closed anterior neural tubes were genotyped. In contrast to the results for control embryos, three of these embryos genotyped as homozygous for the *bug* allele (Figure 7B), indicating that they were rescued. Note also that the example rescued *bug* embryo (yellow arrow) has extra pigment cells, a previously described phenotype of dnEPH3 expression (Haupaix et al., 2014). Finally, we observed a number of embryos that appeared to be partially rescued by dnEPH3 (Figure 7C). These were scored as having open neural tubes for the data shown in Figure 7A.

DISCUSSION

The present study shows a requirement for TTCC signaling in NTC for both ascidians and amphibians, suggesting that this is an ancient function that predates the split of the vertebrates and the tunicates. Zebrafish CAV3.2 is also expressed during neurulation with a partially overlapping pattern to *Xenopus* (http://zfin.org/, probe cb648 [Lewis et al., 2009]). The nature of the defects reported here for loss of T-type Ca^{2+} function in *C. savignyi*, *C. intestinalis*, and *X. laevis* are consistent with it playing a role in the fusion/adhesion of neural folds, rather than in neural specification or neural fold generation. In *C. savignyi* the open anterior neuropore led to a dramatic eruption of the brain from the head of homozygous *bug* mutants. In *X. laevis*, we observed a less frequent, but similar, expulsion of tissue from the open neuropore of CAV3.2 knockdown embryos.

The CAV3 family consists of three vertebrate members (CAV3.1, 3.2, and 3.3) and a single member in tunicates (Perez-Reyes and Lory, 2006; Okamura et al., 2005). This family of Ca^{2+} channels is characterized by rapid opening in response to small membrane depolarizations (Perez-Reyes, 2003). While TTCCs have most thoroughly been investigated in adult tissues such as the heart and neurons, these channels are expressed embryonically (Frischknecht and Randall, 1998; Gottmann

et al., 1988). Recent studies have demonstrated that CAV3.2 in mice initiates differentiation cascades in early embryonic tissues including in neural progenitors, heart, and skeletal muscle (Ferron et al., 2011; Louhivuori et al., 2013; Berthier et al., 2002). It has also been demonstrated that TTCC activity can directly initiate transcriptional programs in chondrocyte differentiation (Lin et al., 2014).

Results presented here show that loss of TTCC function aberrantly upregulates the expression of EphrinA-d and EPHA2, in *C. savignyi* and *X. laevis*, respectively. Although in mouse EphrinA signaling has been reported to promote neural tube fusion (Abdul-Aziz et al., 2009), and loss of ephrinA5 in mice leads to a failure of neural tube fusion (Holmberg et al., 2000), this same pathway in other contexts can lead to cell repulsion (Arvanitis and Davy, 2008). Moreover, results presented here show that overexpression of *ephrinA-d* can lead to an open brain phenotype in *C. savignyi*. Thus, the actions of this pathway (adhesive or repulsive) may depend on the temporal context and/or the relative concentrations. Consistent with this, we observed in *C. savignyi* a spike in *ephrinA-d* expression in the early tail-bud embryo, corresponding to the onset of neural fold fusion. However, by late tail-bud stage, ephrinA-d transcript levels fall dramatically, suggesting that any requirement for ephrinA-d in neural fold fusion is transient. Moreover, the ability of dnEPH3 to rescue *bug* embryos indicates that the downregulation of *ephrinA-d* is necessary for proper anterior neuropore closure.

The CAV3-EphrinA relationship is more complicated in *X. laevis*. While the temporal and spatial expression of all five EphrinA ligands, and ten EphrinA receptors, has not been described, two *X. laevis* EphrinA receptors, EPHA2 and EPHA4, have distinct expression patterns in the neural tube and partially overlap with CAV3.2 expression (Park et al., 2011; Brändli and Kirschner, 1995; Smith et al., 1997) (XDB3, http://Xenopus.nibb.ac.jp). However, there remain many uncharacterized EphrinA ligands and receptors, and the two *Xenopus* TTCCs not examined here, CAV3.1 and CAV3.3, are also expressed at later stages of neural tube closure and are partially redundant with CAV3.2. Redundancy may explain why no NTC defect is reported in the CAV3.2 knockout mouse (Chen et al., 2003). However, the present results suggest that neural fold fusion in these mice should be reexamined.

Finally, CAV3.2-dependent Ca^{2+} transients were observed in the *X. laevis* neural tube. In adult nerve, muscle, and cardiac cells, TTCC activation, and the resulting Ca^{2+} entry, is tied to specific physiological/sensory stimuli (Nelson et al., 2006). However, the embryonic nervous system is characterized by early spontaneous ion channel activity (reviewed in Leclerc et al., 2012; Rosenberg and Spitzer, 2011). Thus, the CAV3.2-dependent Ca^{2+} transients in the closing *Xenopus* neural tube could be the products of either spontaneous activity, or possibly a sensory signaling event. One possible role of TTCCs in NTC could be to monitor the mechanical progress and/or quality of NTC. Interestingly, in adult proprioceptive nerves, CAV3.2 has been found to be essential for low-threshold mechanoreception (François et al., 2015). Future experiments will investigate the potential roles of spontaneous versus sensory activation of TTCCs in NTC.

EXPERIMENTAL PROCEDURES

Ciona Methods

Animals

Adult Ciona were collected from the Santa Barbara Harbor and maintained in constant light in flowing sea water tables. Transgenic lines were maintained at a culturing facility at the University of California, Santa Barbara. Fertilized eggs used for electroporation and transgenesis were collected as previously described (Veeman et al., 2011).

Transgenics and Plasmids

Electroporation methods of *C. intestinalis* and *C. savignyi* were done as previously described (Veeman et al., 2011). The Ciona CRISPR/Cas9 and U6 constructs were used *C. intestinalis* are listed in Table S2, as well as the primer sequences used to detect the CRISPR mediated large deletion ("Mutdet" primers). Construction of a plasmid expressing EphrinA-d under the control of the ETR1 promoter (ETR > EphrinA-d) is detailed in the Supplemental Experimental Procedures. Overexpression of EphrinA-d experiments used 50 μg of ETR > EphrinA-d plasmid and 15 μg of ETR > H2B:GFP. The control experiment used 65 μg of ETR > H2B:GFP. ETR > GCaMP3 was made by similar Gateway methods from an Addgene plasmid of GCaMP3. ETR > GCamP3 was used at 75 μg in *C. savignyi* electroporations.

The dominant-negative EPH3 construct (ETR > dnEPH3) was made using primers (Table S2) to amplify dnEPH3 from Ngn > dnEPH3 (Stolfi et al., 2011). This amplicon was TA cloned into PCR8 (Invitrogen) and then Gateway LR reacted with the ETR > rfa vector (Roure et al., 2007). The resulting plasmid (90 μg) was electroporated into clutches of embryos from heterozygous *bug* parents, as above.

Immunohistochemistry and Imaging

Ciona embryos were fixed in 4% PFA and filtered seawater. CRALBP, Arrestin, and Opsin antibodies were used as previously described in (Tsuda et al., 2003). Anti-PKCzeta antibody was used at 1:300 (Santa Cruz Biotechnology). Washing, secondary staining, and clearing are as previously described (Veeman et al., 2008). Imaging of fixed Ciona samples was either on an Olympus FV1000 confocal or Olympus IX81. Ciona ETR > GCamP3 imaging was on the Olympus IX81 under a 20× water objective. Images were captured every 10 s for 30-min to 1-hr intervals starting from neurula stages and ending in late tail-bud stages of *C. savignyi*. Calcium transients were analyzed and quantified on Image J. In situ hybridizations were imaged on an Olympus BX51 with DIC optics and 20× objective. Fluorescent in situ hybridizations were cleared in glycerol and imaged on an Olympus FV1000 confocal under a 20× objective.

RT-PCR

C. savignyi bug mutants and wild-type siblings larvae were collected for RNA as previously described (Abdul-Wajid et al., 2014). For comparisons of mutant and wild-type by qRT-PCR, equal amounts of total RNA used in each PCR and run as biological and technical triplicates. For the qPCR developmental time course, equal amounts of RNA were used for cDNA synthesis at each time point (200 ng). Primers for qPCR are listed in Table S2.

For single tadpole Ciona genomic PCR, genomic DNA was isolated as previously described (Veeman et al., 2011), and primers are listed in Table S2.

Drug Treatments

Mibefradil dihydrochloride (Sigma-Aldrich) was reconstituted at 4 mM in filtered water and stored at 4°C degrees. Nifedipine was used as previously described (Hackley et al., 2013), and equivalent amounts of DMSO were used as control in this experiment. Experimental concentrations were diluted in filtered seawater with antibiotics (streptomycin and kanamycin) in a 3-cm petri dish to which embryos of the appropriate stage were added. Embryos were washed of drug at the indicated stage through three changes of filtered seawater and allowed to develop in a new petri dish of filtered seawater and antibiotics.

Xenopus Methods

Animals

Females were induced for ovulation by a subcutaneous injection of human chorionic gonadotropin hormone as described (Sive et al., 2007). Eggs and sperm were collected for in vitro fertilization as described (Sive et al., 2000). Animal care and use were in accordance with regulations established by the Institutional Animal Care and Use Committee at the University of California, Santa Barbara.

Morpholino Injections

X. laevis CAV3.2 morpholinos (MOs) were designed according to the sequence of GenBank entry GQ120631 and alignment with scaffold 22599 in *X. laevis* genome v.6 (http://www.xenbase.org/entry/). Two controls were used: the standard control morpholino (Gene Tools, CTL MO1) and a mismatch MO containing a 5-bp mismatch from CAV3.2 splice disrupting morpholino 1 (CTL-MO2). Sequences for both CAV3.2 MOs and CAV3.2 mismatch MOs are in Table S1.

Fertilized eggs were microinjected MOs at final doses of 40, 20, and 10 ng in a 10-nl drop. After dose determination, subsequent embryos used for coronal section imaging or RNA isolation were injected with a combination of CAV3.2 MO1 and MO2 at 40 ng final, or the CTL-MO2 at the same concentration. The same combination and concentrations of MOs were used in the GCamP3 co-injection experiments. The embryos were imaged for developmental defects from neurula to tail-bud stages and then fixed in 4% paraformaldehyde + MEM for immunohistochemistry or lysed in Trizol for RT-PCR analysis (Blackiston et al., 2010). RNAs for GCaMP3 were made from a gene construct using the T3 mMessage in vitro Transcription kit (Ambion), and 1 ng of RNA was co-injected with the MOs as indicated.

Immunohistochemistry and Imaging

X. laevis embryos were fixed, embedded, and sectioned as described (Blackiston et al., 2010). Primary antibody sera to NCAM (4d-s) and E-cadherin (5D3) were obtained from the Developmental Studies Hybridoma Bank at University of Iowa and used at final concentrations of 5 μg/ml. Fluorophore-conjugated secondary antibodies (Invitrogen) were used at 1:500. Sections were mounted in glycerol.

For GCamP3 imaging, GFP-expressing embryos from each experimental condition were placed in 1% low melting pointing agarose and 1/3 × MMR on a coverslip-bottom dish. Embryos were oriented with neural plates facing down and then imaged on an inverted Zeiss 780 LSM or an Olympus FV1000. Imaging was done with a 20× objective, and images were captured every second for 8–10 min. The analysis of GCamP3 images was done with ImageJ and described in the Supplemental Experimental Procedures.

RT-PCR

Primers used for RT-PCR on *X. laevis* single tadpole cDNA are listed in Table S2. Single embryos were lysed in TRIZOL for RNA isolation, and 400 ng of total RNA was used to make cDNA (Invitrogen Superscript III).

SUPPLEMENTAL INFORMATION

Supplemental Information includes Supplemental Experimental Procedures, two figures, two tables, and five movies and can be found with this article online at http://dx.doi.org/10.1016/j.celrep.2015.09.035.

AUTHOR CONTRIBUTIONS

S.A.-W. and W.C.S. conceived and designed experiments. S.A.-W., H.M.-D., and S.M.K. performed experiments. S.A.-W. and W.C.S. wrote the paper.

ACKNOWLEDGMENTS

We thank Erin Newman-Smith, Eli Spina, and Matt Kourakis for their critical reading of this manuscript. We also thank Jasmine Anderson for her efforts in cloning the *C. intestinalis* guide RNA constructs and Alberto Stolfi for sharing CRISPR and dnEPH3 plasmids. This work was supported by award HD038701 from the NIH to W.C.S.

Received: April 28, 2015
Revised: August 6, 2015
Accepted: September 11, 2015
Published: October 15, 2015

REFERENCES

Abdul-Aziz, N.M., Turmaine, M., Greene, N.D., and Copp, A.J. (2009). EphrinA-EphA receptor interactions in mouse spinal neurulation: implications for neural fold fusion. Int. J. Dev. Biol. *53*, 559–568.

Abdul-Wajid, S., Veeman, M.T., Chiba, S., Turner, T.L., and Smith, W.C. (2014). Exploiting the extraordinary genetic polymorphism of ciona for developmental genetics with whole genome sequencing. Genetics *197*, 49–59.

Arvanitis, D., and Davy, A. (2008). Eph/ephrin signaling: networks. Genes Dev. *22*, 416–429.

Berthier, C., Monteil, A., Lory, P., and Strube, C. (2002). Alpha(1H) mRNA in single skeletal muscle fibres accounts for T-type calcium current transient expression during fetal development in mice. J. Physiol. *539*, 681–691.

Blackiston, D., Vandenberg, L.N., and Levin, M. (2010). High-throughput Xenopus laevis immunohistochemistry using agarose sections. Cold Spring Harb. Protoc. *2010*, t5532.

Brändli, A.W., and Kirschner, M.W. (1995). Molecular cloning of tyrosine kinases in the early Xenopus embryo: identification of Eck-related genes expressed in cranial neural crest cells of the second (hyoid) arch. Dev. Dyn. *203*, 119–140.

Bronner-Fraser, M., Wolf, J.J., and Murray, B.A. (1992). Effects of antibodies against N-cadherin and N-CAM on the cranial neural crest and neural tube. Dev. Biol. *153*, 291–301.

Chen, C.C., Lamping, K.G., Nuno, D.W., Barresi, R., Prouty, S.J., Lavoie, J.L., Cribbs, L.L., England, S.K., Sigmund, C.D., Weiss, R.M., et al. (2003). Abnormal coronary function in mice deficient in alpha1H T-type Ca2+ channels. Science *302*, 1416–1418.

Deschet, K., and Smith, W.C. (2004). Frimousse–a spontaneous ascidian mutant with anterior ectodermal fate transformation. Curr. Biol. *14*, R408–R410.

Ferron, L., Ruchon, Y., Renaud, J.F., and Capuano, V. (2011). T-type Ca^{2+} signalling regulates aldosterone-induced CREB activation and cell death through PP2A activation in neonatal cardiomyocytes. Cardiovasc. Res. *90*, 105–112.

François, A., Schüetter, N., Laffray, S., Sanguesa, J., Pizzoccaro, A., Dubel, S., Mantilleri, A., Nargeot, J., Noël, J., Wood, J.N., et al. (2015). The low-threshold calcium channel Cav3.2 determines low-threshold mechanoreceptor function. Cell Rep. *10*, 370–382.

Frischknecht, F., and Randall, A.D. (1998). Voltage- and ligand-gated ion channels in floor plate neuroepithelia of the rat. Neuroscience *85*, 1135–1149.

Ghosh, S., Marquardt, T., Thaler, J.P., Carter, N., Andrews, S.E., Pfaff, S.L., and Hunter, T. (2008). Instructive role of aPKCzeta subcellular localization in the assembly of adherens junctions in neural progenitors. Proc. Natl. Acad. Sci. USA *105*, 335–340.

Gottmann, K., Dietzel, I.D., Lux, H.D., Huck, S., and Rohrer, H. (1988). Development of inward currents in chick sensory and autonomic neuronal precursor cells in culture. J. Neurosci. *8*, 3722–3732.

Greene, N.D., and Copp, A.J. (2014). Neural tube defects. Annu. Rev. Neurosci. *37*, 221–242.

Hackley, C., Mulholland, E., Kim, G.J., Newman-Smith, E., and Smith, W.C. (2013). A transiently expressed connexin is essential for anterior neural plate development in Ciona intestinalis. Development *140*, 147–155.

Haigo, S.L., Hildebrand, J.D., Harland, R.M., and Wallingford, J.B. (2003). Shroom induces apical constriction and is required for hingepoint formation during neural tube closure. Curr. Biol. *13*, 2125–2137.

Harrington, M.J., Hong, E., and Brewster, R. (2009). Comparative analysis of neurulation: first impressions do not count. Mol. Reprod. Dev. *76*, 954–965.

Haupaix, N., Stolfi, A., Sirour, C., Picco, V., Levine, M., Christiaen, L., and Yasuo, H. (2013). p120RasGAP mediates ephrin/Eph-dependent attenuation of FGF/ERK signals during cell fate specification in ascidian embryos. Development *140*, 4347–4352.

Haupaix, N., Abitua, P.B., Sirour, C., Yasuo, H., Levine, M., and Hudson, C. (2014). Ephrin-mediated restriction of ERK1/2 activity delimits the number of pigment cells in the Ciona CNS. Dev. Biol. *394*, 170–180.

Holmberg, J., Clarke, D.L., and Frisén, J. (2000). Regulation of repulsion versus adhesion by different splice forms of an Eph receptor. Nature *408*, 203–206.

Hotta, K., Mitsuhara, K., Takahashi, H., Inaba, K., Oka, K., Gojobori, T., and Ikeo, K. (2007). A web-based interactive developmental table for the ascidian

Ciona intestinalis, including 3D real-image embryo reconstructions: I. From fertilized egg to hatching larva. Dev. Dyn. *236*, 1790–1805.

Imai, K.S., Stolfi, A., Levine, M., and Satou, Y. (2009). Gene regulatory networks underlying the compartmentalization of the Ciona central nervous system. Development *136*, 285–293.

Ji, Y.J., Hwang, Y.S., Mood, K., Cho, H.J., Lee, H.S., Winterbottom, E., Cousin, H., and Daar, I.O. (2014). EphrinB2 affects apical constriction in Xenopus embryos and is regulated by ADAM10 and flotillin-1. Nat. Commun. *5*, 3516.

Jiang, D., Tresser, J.W., Horie, T., Tsuda, M., and Smith, W.C. (2005). Pigmentation in the sensory organs of the ascidian larva is essential for normal behavior. J. Exp. Biol. *208*, 433–438.

Leclerc, C., Néant, I., and Moreau, M. (2012). The calcium: an early signal that initiates the formation of the nervous system during embryogenesis. Front. Mol. Neurosci. *5*, 3.

Lewis, B.B., Wester, M.R., Miller, L.E., Nagarkar, M.D., Johnson, M.B., and Saha, M.S. (2009). Cloning and characterization of voltage-gated calcium channel alpha1 subunits in Xenopus laevis during development. Dev. Dyn. *238*, 2891–2902.

Lin, S.S., Tzeng, B.H., Lee, K.R., Smith, R.J., Campbell, K.P., and Chen, C.C. (2014). Cav3.2 T-type calcium channel is required for the NFAT-dependent Sox9 expression in tracheal cartilage. Proc. Natl. Acad. Sci. USA *111*, E1990–E1998.

Louhivuori, L.M., Louhivuori, V., Wigren, H.K., Hakala, E., Jansson, L.C., Nordström, T., Castrén, M.L., and Akerman, K.E. (2013). Role of low voltage activated calcium channels in neuritogenesis and active migration of embryonic neural progenitor cells. Stem Cells Dev. *22*, 1206–1219.

Manni, L., Agnoletto, A., Zaniolo, G., and Burighel, P. (2005). Stomodeal and neurohypophysial placodes in Ciona intestinalis: insights into the origin of the pituitary gland. J. Exp. Zoolog. B Mol. Dev. Evol. *304*, 324–339.

Martin, R.L., Lee, J.H., Cribbs, L.L., Perez-Reyes, E., and Hanck, D.A. (2000). Mibefradil block of cloned T-type calcium channels. J. Pharmacol. Exp. Ther. *295*, 302–308.

Murdoch, J.N., Doudney, K., Paternotte, C., Copp, A.J., and Stanier, P. (2001). Severe neural tube defects in the loop-tail mouse result from mutation of Lpp1, a novel gene involved in floor plate specification. Hum. Mol. Genet. *10*, 2593–2601.

Nelson, M.T., Todorovic, S.M., and Perez-Reyes, E. (2006). The role of T-type calcium channels in epilepsy and pain. Curr. Pharm. Des. *12*, 2189–2197.

Nishida, H. (1987). Cell lineage analysis in ascidian embryos by intracellular injection of a tracer enzyme. III. Up to the tissue restricted stage. Dev. Biol. *121*, 526–541.

Okamura, Y., Nishino, A., Murata, Y., Nakajo, K., Iwasaki, H., Ohtsuka, Y., Tanaka-Kunishima, M., Takahashi, N., Hara, Y., Yoshida, T., et al. (2005). Comprehensive analysis of the ascidian genome reveals novel insights into the molecular evolution of ion channel genes. Physiol. Genomics *22*, 269–282.

Olinski, R.P., Dahlberg, C., Thorndyke, M., and Hallböök, F. (2006). Three insulin-relaxin-like genes in Ciona intestinalis. Peptides *27*, 2535–2546.

Park, E.C., Cho, G.S., Kim, G.H., Choi, S.C., and Han, J.K. (2011). The involvement of Eph-Ephrin signaling in tissue separation and convergence during Xenopus gastrulation movements. Dev. Biol. *350*, 441–450.

Perez-Reyes, E. (2003). Molecular physiology of low-voltage-activated t-type calcium channels. Physiol. Rev. *83*, 117–161.

Perez-Reyes, E., and Lory, P. (2006). Molecular biology of T-type calcium channels. CNS Neurol. Disord. Drug Targets *5*, 605–609.

Picco, V., Hudson, C., and Yasuo, H. (2007). Ephrin-Eph signalling drives the asymmetric division of notochord/neural precursors in Ciona embryos. Development *134*, 1491–1497.

Pyrgaki, C., Liu, A., and Niswander, L. (2011). Grainyhead-like 2 regulates neural tube closure and adhesion molecule expression during neural fold fusion. Dev. Biol. *353*, 38–49.

Raible, F., and Brand, M. (2004). Divide et Impera–the midbrain-hindbrain boundary and its organizer. Trends Neurosci. *27*, 727–734.

Ran, F.A., Hsu, P.D., Wright, J., Agarwala, V., Scott, D.A., and Zhang, F. (2013). Genome engineering using the CRISPR-Cas9 system. Nat. Protoc. *8*, 2281–2308.

Rosenberg, S.S., and Spitzer, N.C. (2011). Calcium signaling in neuronal development. Cold Spring Harb. Perspect. Biol. *3*, a004259.

Roure, A., Rothbächer, U., Robin, F., Kalmar, E., Ferone, G., Lamy, C., Missero, C., Mueller, F., and Lemaire, P. (2007). A multicassette Gateway vector set for high throughput and comparative analyses in ciona and vertebrate embryos. PLoS ONE *2*, e916.

Sive, H.L., Grainger, R.M., and Harland, R.M. (2000). Early Development of Xenopus laevis: A Laboratory Manual (Cold Spring Harbor Laboratory Press).

Sive, H.L., Grainger, R.M., and Harland, R.M. (2007). Inducing ovulation in *Xenopus laevis*. CSH Protoc *2007*, t4734.

Smith, A., Robinson, V., Patel, K., and Wilkinson, D.G. (1997). The EphA4 and EphB1 receptor tyrosine kinases and ephrin-B2 ligand regulate targeted migration of branchial neural crest cells. Curr. Biol. *7*, 561–570.

Solecki, D.J., Govek, E.E., Tomoda, T., and Hatten, M.E. (2006). Neuronal polarity in CNS development. Genes Dev. *20*, 2639–2647.

Stolfi, A., Wagner, E., Taliaferro, J.M., Chou, S., and Levine, M. (2011). Neural tube patterning by Ephrin, FGF and Notch signaling relays. Development *138*, 5429–5439.

Stolfi, A., Gandhi, S., Salek, F., and Christiaen, L. (2014). Tissue-specific genome editing in Ciona embryos by CRISPR/Cas9. Development *141*, 4115–4120.

Takamura, K., Oka, N., Akagi, A., Okamoto, K., Okada, T., Fukuoka, T., Hogaki, A., Naito, D., Oobayashi, Y., and Satoh, N. (2001). EST analysis of genes that are expressed in the neural complex of Ciona intestinalis adults. Zoolog. Sci. *18*, 1231–1236.

Tian, L., Hires, S.A., Mao, T., Huber, D., Chiappe, M.E., Chalasani, S.H., Petreanu, L., Akerboom, J., McKinney, S.A., Schreiter, E.R., et al. (2009). Imaging neural activity in worms, flies and mice with improved GCaMP calcium indicators. Nat. Methods *6*, 875–881.

Tresser, J., Chiba, S., Veeman, M., El-Nachef, D., Newman-Smith, E., Horie, T., Tsuda, M., and Smith, W.C. (2010). doublesex/mab3 related-1 (dmrt1) is essential for development of anterior neural plate derivatives in Ciona. Development *137*, 2197–2203.

Tsuda, M., Kusakabe, T., Iwamoto, H., Horie, T., Nakashima, Y., Nakagawa, M., and Okunou, K. (2003). Origin of the vertebrate visual cycle: II. Visual cycle proteins are localized in whole brain including photoreceptor cells of a primitive chordate. Vision Res. *43*, 3045–3053.

Veeman, M.T., Nakatani, Y., Hendrickson, C., Ericson, V., Lin, C., and Smith, W.C. (2008). Chongmague reveals an essential role for laminin-mediated boundary formation in chordate convergence and extension movements. Development *135*, 33–41.

Veeman, M.T., Newman-Smith, E., El-Nachef, D., and Smith, W.C. (2010). The ascidian mouth opening is derived from the anterior neuropore: reassessing the mouth/neural tube relationship in chordate evolution. Dev. Biol. *344*, 138–149.

Veeman, M.T., Chiba, S., and Smith, W.C. (2011). Ciona genetics. Methods Mol. Biol. *770*, 401–422.

Wallingford, J.B. (2005). Neural tube closure and neural tube defects: studies in animal models reveal known knowns and known unknowns. Am. J. Med. Genet. C. Semin. Med. Genet. *135C*, 59–68.

Wallingford, J.B., and Harland, R.M. (2001). Xenopus Dishevelled signaling regulates both neural and mesodermal convergent extension: parallel forces elongating the body axis. Development *128*, 2581–2592.

Wallingford, J.B., Niswander, L.A., Shaw, G.M., and Finnell, R.H. (2013). The continuing challenge of understanding, preventing, and treating neural tube defects. Science *339*, 1222002.

Ybot-Gonzalez, P., and Copp, A.J. (1999). Bending of the neural plate during mouse spinal neurulation is independent of actin microfilaments. Dev. Dyn. *215*, 273–283.